# Optical Imaging and Spectroscopic Characterization of Self-Assembled Environmental Adsorbates on Graphene

Patrick Gallagher,<sup>†</sup> Yilei Li,<sup>‡</sup> Kenji Watanabe,<sup>§</sup> Takashi Taniguchi,<sup>§</sup> Tony F. Heinz,\*,<sup>‡</sup> and David Goldhaber-Gordon\*,<sup>†</sup>

†Department of Physics, Stanford University, Stanford, CA 94305, USA

‡Department of Applied Physics, Stanford University, Stanford, CA 94305, USA

¶SLAC National Accelerator Laboratory, 2575 Sand Hill Rd, Menlo Park, CA 94025, USA

§National Institute for Materials Science, 1-1 Namiki, Tsukuba, 305-0044, Japan

E-mail: tony.heinz@stanford.edu; goldhaber-gordon@stanford.edu

#### Abstract

Topographic studies using scanning probes have found that graphene surfaces are often covered by micron-scale domains of periodic stripes with a 4 nm pitch. These stripes have been variously interpreted as structural ripples or as self-assembled adsorbates. We show that the stripe domains are optically anisotropic by imaging them using a polarization-contrast technique. Optical spectra between 1.1 and 2.8 eV reveal that the anisotropy in the in-plane dielectric function is predominantly real, reaching 0.6 for an assumed layer thickness of 0.3 nm. The spectra are incompatible with a rippled graphene sheet, but would be quantitatively explained by the self-assembly of chain-like organic molecules into nanoscale stripes.

# **Keywords**

graphene, adsorbates, self-assembly, polarized light, friction

Isolated graphene must buckle out of its plane to achieve thermodynamic stability. <sup>1</sup> This intrinsic rippling is apparently suppressed when graphene is supported on a flat substrate, as topographic images of graphene on atomically flat mica, for instance, have revealed a textureless, isotropic surface. <sup>2</sup> Yet friction-force microscopy images of supported graphene sheets have surprisingly also revealed domains of strongly anisotropic friction, <sup>3</sup> suggesting the presence of a symmetry-breaking texture. Recent topographic measurements using high-resolution atomic force microscopy (AFM) have directly imaged this texture: periodic nanoscale stripes (period 4 nm, amplitude  $\sim 0.1$  nm) were found to fully cover the surfaces of graphene flakes supported on a variety of substrates, including atomically flat hexagonal boron nitride (hBN). <sup>4,5</sup> These stripes are oriented along one of the three armchair axes of the underlying graphene crystal and form micron-scale orientational domains whose friction signal is strongly anisotropic. <sup>4</sup> The topographic or frictional signatures of these nanoscale stripes have been observed on graphene by several groups, <sup>3-6</sup> and similar phenomena have been reported on graphite, <sup>7-10</sup> hBN, <sup>4</sup> and molybdenum disulfide. <sup>11</sup>

Owing to the lack of chemical sensitivity in the existing scanning probe measurements, the identity of these stripes remains a matter of debate. While some have proposed that the stripes are structural features of the crystals themselves,  $^{3,5,11}$  we have argued in a previous publication that the stripes are self-assembled molecules from an unidentified environmental source,  $^4$  and others have more specifically claimed that the stripes are composed of nitrogen or oxygen molecules.  $^{6-8}$  In this Letter, we study the stripes on graphene using polarized light, which has been used to sensitively measure optical anisotropy in materials ranging from bulk crystals  $^{12,13}$  to carbon nanotubes  $^{14,15}$  and molecular monolayers.  $^{16}$  The polarized images of graphene reveal optically anisotropic domains matching those observed in friction images. The measured anisotropy  $\Delta\epsilon$  in the in-plane dielectric function is almost entirely real at visible and near-infrared wavelengths, incompatible with expectations for a rippled

graphene sheet, but consistent with a self-assembled molecular layer. While our experiment does not directly identify the chemical species forming the stripes, an ordered monolayer of organic chain molecules—known to self-assemble into nanoscale stripes on the basal plane of graphite  $^{17-19}$  and graphene  $^{20-23}$ —would explain the sign and magnitude of  $\Delta\epsilon$ .

Since the overall optical response of our substrate-supported graphene samples is predominantly isotropic, we use a polarization-contrast microscopy technique to enhance the visibility of the stripe-induced optical anisotropy. In our apparatus (Fig. 1a), incident light passes through a polarizer and is directed onto the sample at normal incidence. Light reflected by the sample passes through a rotatable polarization analyzer before being collected by a camera. The analyzer is nearly orthogonal to the polarizer, deviating only by a small angle  $\delta$  (Fig. 1b); this widely used arrangement <sup>12–16</sup> greatly suppresses the isotropic optical response without significantly diminishing the anisotropic response. We note that small anisotropies are sometimes measured by modulating the incident polarization and detecting the time-varying signal (reflection anisotropy spectroscopy <sup>24</sup>); our apparatus is much simpler, but nonetheless provides high sensitivity to optical anisotropy. To quantify this claim, we may decompose the reflection coefficients along the principal axes of optical anisotropy  $\hat{x}$  and  $\hat{y}$  into an isotropic part r and an anisotropic part  $\beta$ :  $r_x = r + \beta$  and  $r_y = r - \beta$ . An analysis (Supporting Information) of the polarization state assuming  $|r| \gg |\beta|$  finds the detected intensity to be  $I \propto |r|^2 - 2\text{Re}\{r^*\beta\}\sin(2\theta - \delta)/\sin\delta$ , where  $\theta$  is the angle between  $\hat{x}$ and the polarizer (Fig. 1b). The anisotropic term is enhanced relative to the isotropic term by the factor  $\sin(2\theta - \delta)/\sin\delta$ , which approaches 30 for experimentally reasonable values  $\delta = 2^{\circ}$  and  $\theta = 45^{\circ}$ .

This relative enhancement modifies the measured optical contrast  $C = (I_{\text{flake}} - I_{\text{sub}})/I_{\text{sub}}$ between a flake and bare substrate to be more sensitive to the anisotropy (hence our term "polarization-contrast" microscopy). Here  $I_{\text{flake}}$  and  $I_{\text{sub}}$  are the detected intensities reflected from flake-covered and bare substrate. The contrast can be written as (Supporting Informa-

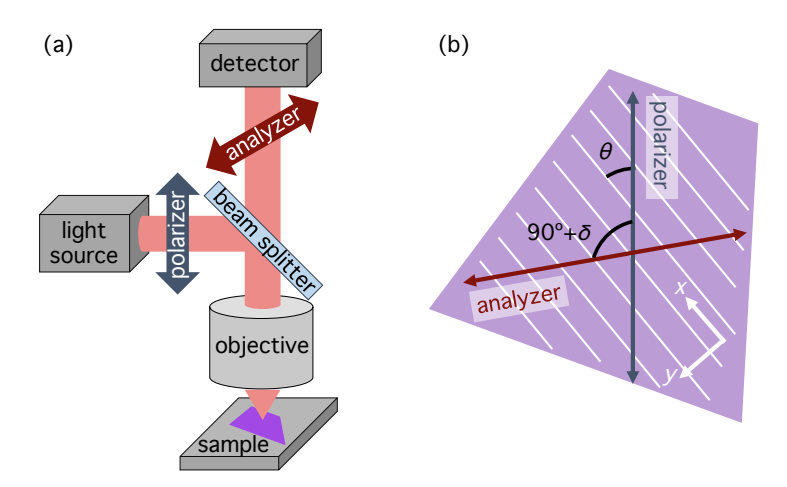


Figure 1: Polarization-contrast microscopy. (a) Microscopy apparatus. Incident light passes through a polarizer and is focused onto the sample by an objective. Light reflected by the sample passes through a rotatable analyzer before being detected by a camera or spectrometer. (b) Relative orientations of polarizer, analyzer, and principal axes  $\hat{x}$  and  $\hat{y}$  of the anisotropic layer;  $\hat{x}$  (white lines) makes an angle  $\theta$  with the transmission axis of the polarizer.

tion)
$$C = C_{\text{unpol}} - \frac{\pi d}{\lambda} \text{Im} \left\{ \Delta \epsilon F_{\text{sub}} \right\} \frac{\sin(2\theta - \delta)}{\sin \delta}, \tag{1}$$

where  $C_{\rm unpol}$  is the contrast of the flake when viewed with unpolarized light,  $^{25}$   $F_{\rm sub} \equiv (1 + r_{\rm sub})^2/r_{\rm sub}$  is a function of the substrate reflection coefficient  $r_{\rm sub}$ , and  $\Delta \epsilon = \epsilon_x - \epsilon_y$  is the anisotropy of the in-plane dielectric function of the flake and/or its molecular overlayer. We use the convention that the electric field  $E \propto e^{i\omega t}$ , and we expand to first order in  $\Delta \epsilon$  since the effective thickness d of the anisotropic layer is much smaller than the wavelength  $\lambda$ . Eq. 1 shows that the contrast should deviate from its unpolarized value by a term containing  $\Delta \epsilon$  and the aforementioned enhancement factor of  $\sin(2\theta - \delta)/\sin\delta$ .

Monolayer graphene samples used in this study were deposited under ambient conditions by tape-assisted mechanical exfoliation onto oxidized silicon wafers. Without further processing of the samples following exfoliation, friction-force images revealed micron-scale domains of anisotropic friction<sup>3,4</sup> fully covering the flakes (Fig. 2b). The friction signal of each domain is two-fold symmetric under rotation, and the local axis of high friction is known<sup>4,26</sup> to be aligned with one of three armchair axes of graphene. Tapping-mode AFM

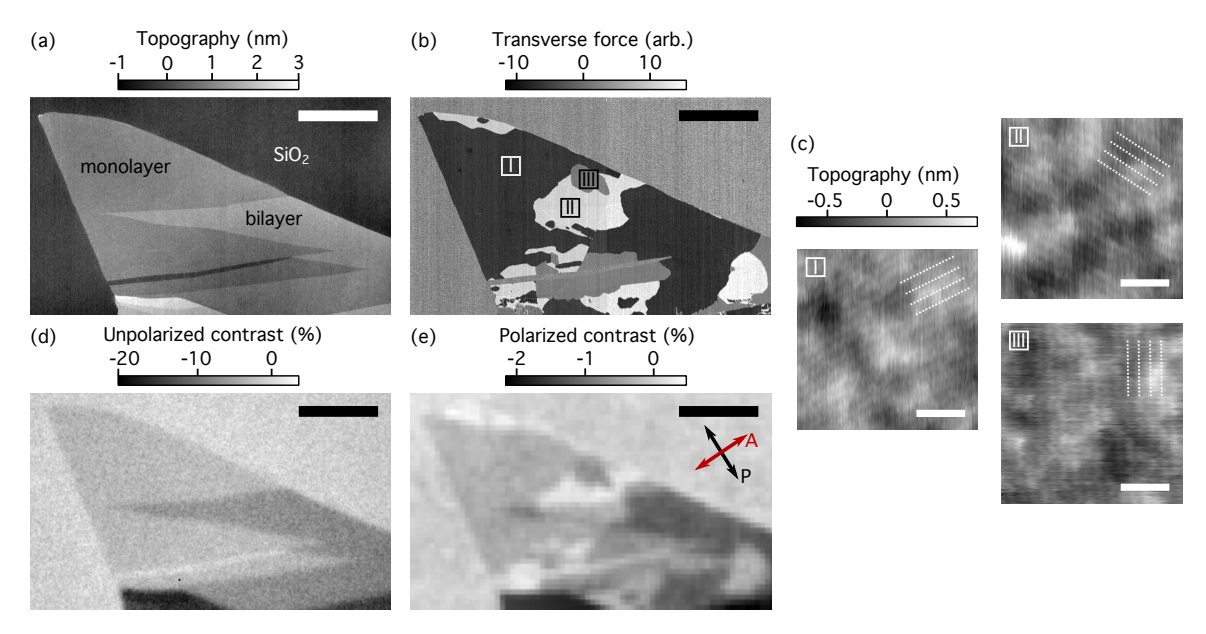


Figure 2: Polarization-contrast microscopy of striped graphene. **a**, Contact AFM topography scan of a graphene flake (Sample A) supported on 302 nm of silicon oxide on silicon. Scale bar is 10  $\mu$ m. **b**, Simultaneously recorded transverse force signal showing domains of anisotropic friction with three distinct axes of anisotropy, labeled as domains I, II, and III. **c**, Tapping mode AFM showing stripe axes in domains I, II, and III. Stripe period is  $4.5 \pm 0.2$  nm. Scale bars are 20 nm. **d**, Unpolarized optical image of the same flake illuminated with white light and observed using the green channel of our camera. **e**, Polarization-contrast image (green channel) with  $\delta = 2^{\circ}$ . Inset diagram shows the orientations of polarizer (P) and analyzer (A).

topography scans show that the origin of these frictional domains is an array of nanoscale stripes with a period of approximately 4 nm and a measured amplitude  $\sim 0.1$  nm (Fig. 2c). The flakes that we studied appear to be uniformly covered with stripes, with no evidence of thicker or thinner regions that might suggest multilayer coverage of adsorbates. A detailed discussion of the stripes and the conditions under which they form can be found in Ref. 4.

While the domains are invisible in the ordinary, unpolarized, optical image (Fig. 2d), they are readily observed in the polarization-contrast image with  $\delta \approx 2^{\circ}$  (Fig. 2e), acquired using a Nikon LV100 polarizing microscope. Three groups of domains with distinct values of contrast can be identified, forming spatial patterns matching those in the friction image (Fig. 2b). The domain contrast appears to overlay on top of the unpolarized optical contrast  $C_{\rm unpol}$ , in agreement with Eq. 1. Domain contrast is maximized in the green channel of our microscope owing to the photon energy dependence of  $F_{\rm sub}$  (see Eq. 1). We note that  $C_{\rm unpol}$  in the polarization-contrast image (Fig. 2e) is less than half its value for the unpolarized image (Fig. 2d); this is an experimental artifact resulting from stray light or dark counts in the camera, which reduce the contrast by making spurious contributions to the measured intensity.

Rotating the sample while holding the polarizers fixed changes the relative contrast of the domains (see Supporting Movie). Once per half revolution, each group of domains with a particular stripe axis will appear dark, while the other two groups appear bright (Fig. 3, upper panels). The contrast of a given domain evolves sinusoidally, completing two periods in one full revolution of the sample, with phase offset by  $\pm 60^{\circ}$  from the contrast sinusoids of the other two domains (Fig. 3, lower panel). The average contrast is offset to approximately -1%. This behavior follows Eq. 1: the contrast should evolve as  $\sin(2\theta - \delta) \approx \sin 2\theta$  with an average shift from zero arising from  $C_{\text{unpol}}$ . The sinusoidal part vanishes when the principal axis is parallel or orthogonal to the polarizer, making  $\theta$  an integer multiple of 90°. We observe the sinusoidal part to vanish when the polarizer is aligned with or perpendicular to the stripe axis measured in AFM (vertical bars in Fig. 3, lower panel), implying that the

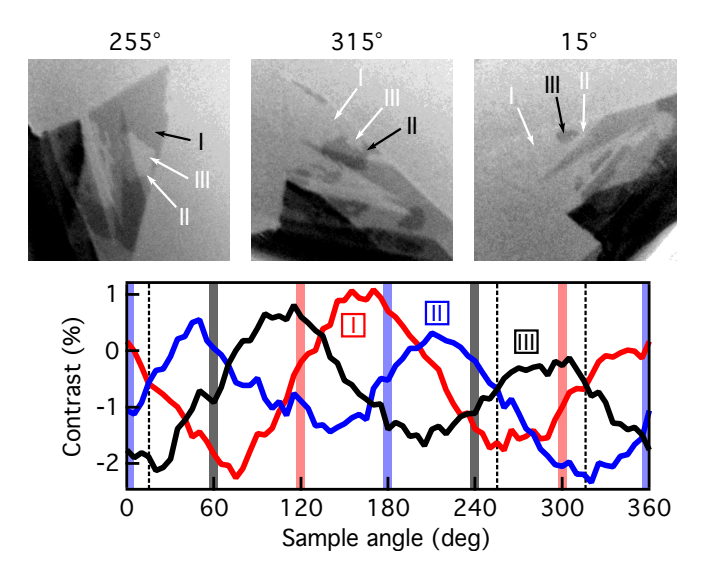


Figure 3: Contrast variation with sample rotation. Top: images of Sample A for different sample rotation angles, with the polarizer fixed along the horizontal and the analyzer held nearly vertical ( $\delta=2^{\circ}$ ). At sample angles 255°, 315°, and 15°, domains labeled I, II, and III (respectively) in Fig. 2 are dark, while the other two domains are equally bright. Bottom: measured contrast of domains I, II, and III (red, black, and blue curves, respectively) as a function of sample angle. Color-coded vertical bars indicate the sample angles at which each stripe axis measured by AFM aligns with the polarizer (width of bar indicates uncertainty in AFM measurement); the offset of sample angle is chosen such that the polarizer aligns with one of the stripe axes when the sample angle is an integer multiple of 60°. Dashed vertical lines mark the sample angles 255°, 315°, and 15°, which correspond to the images above. All images and contrast data shown are collected using the green channel of our camera.

principal axes of a given domain are parallel and perpendicular to the stripe axis.

We quantitatively measured Re $\{\Delta\epsilon\}$  and Im $\{\Delta\epsilon\}$  as a function of photon energy for two monolayer graphene samples (A and B) using a home-built microscope (layout shown in Fig. 1a) equipped with a spectrometer and a supercontinuum laser (Fianium, 0.8 to 2.8 eV) supplying broadband illumination. Calcite-based polarizers (Thorlabs GT10) give the apparatus a high polarization extinction ratio (> 30,000). For both samples, we collected contrast spectra versus analyzer angle  $\delta$  at two different sample rotations  $\theta$  with the laser spot placed within a specific domain. The precise value of  $\theta$  is determined from AFM measurements of the stripes, which are parallel to  $\hat{x}$  (Fig. 1b).

For small  $\delta$ , the contrast should diverge like  $\delta^{-1}$  with a coefficient proportional to Im  $\{\Delta \epsilon F_{\rm sub}\}$  (Eq. 1). If  $F_{\rm sub}$  is purely imaginary or purely real—as is the case for several energies within our spectral range (Fig. 4a)—the coefficient of the  $\delta^{-1}$  behavior will thus be proportional to Re $\{\Delta \epsilon\}$  or Im $\{\Delta \epsilon\}$ , respectively. At all photon energies for which  $F_{\rm sub}$  is purely imaginary (~1.2, 1.6, 2.7 eV), the contrast exhibits a clear  $\delta^{-1}$  dependence (Fig. 4b and Supporting Information) except for  $|\delta| \lesssim 1^{\circ}$ , where the behavior is governed by imperfections in the apparatus (discussed below). We conclude that Re $\{\Delta \epsilon\}$  is appreciable at these energies. On the other hand, at photon energies for which  $F_{\rm sub}$  is purely real (~1.4, 2.1 eV), the contrast does not vary as  $\delta^{-1}$ , instead remaining nearly flat aside from a symmetric peak or dip for  $|\delta| \lesssim 1^{\circ}$  (Fig. 4c and Supporting Information). The absence of a  $\delta^{-1}$  component at these energies implies that Im $\{\Delta \epsilon\}$  is small. Provided that  $\Delta \epsilon$  varies sufficiently slowly with energy, these observations suggest that  $\Delta \epsilon$  is predominantly real throughout our spectral range, as confirmed more thoroughly below.

The deviation from Eq. 1 for  $|\delta| \lesssim 1^{\circ}$  results from an unintentional, strain-induced birefringence in our objective, which induces a phase shift  $\eta$  between transmitted waves polarized along the two principal axes of the objective. (A polarization-dependent phase shift for light reflected by or transmitted through the beamsplitter would lead to a similar effect. We have verified that for our beamsplitter, which is a glass piece carefully mounted to min-

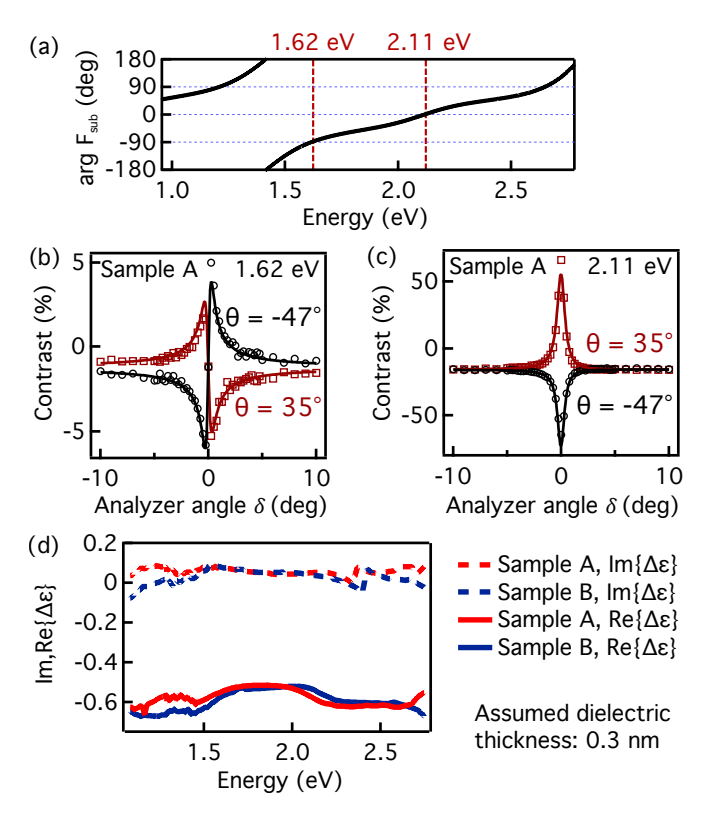


Figure 4: Quantitative determination of the dielectric anisotropy for striped graphene on oxidized silicon. (a) Complex argument of  $F_{\rm sub}$  for 302 nm of silicon oxide on silicon, the substrate used for Sample A, calculated using a thin film model (Supporting Information). Dashed vertical lines indicate energies for which  $\arg F_{\rm sub}$  is either purely real or purely imaginary. (b) Contrast versus analyzer angle  $\delta$  for a single stripe domain on Sample A in two different rotational orientations  $\theta$  with respect to the polarizer. Photon energy is 1.62 eV, for which  $F_{\rm sub}$  is purely imaginary. (c) Contrast data and fits for Sample A in the same orientations, but for a photon energy of 2.11 eV, for which  $F_{\rm sub}$  is purely real. (d)  $\mathrm{Re}\{\Delta\epsilon\}$  (solid lines) and  $\mathrm{Im}\{\Delta\epsilon\}$  (dashed lines) extracted from the contrast fits for Samples A and B at all accessible energies.

imize strain, this phase shift is negligible compared to that of the objective.) A calculation incorporating the phase shift  $\eta$  (Supporting Information) reveals that for sufficiently small  $\delta$ , instead of continuing to diverge as  $\delta^{-1}$ , the contrast saturates to a finite value proportional to  $\eta^{-1}\text{Re}\{\Delta\epsilon F_{\text{sub}}\}\sin 2\theta$ . Given  $\eta$ , a fit to the expression for the contrast with a strained objective thus yields both  $\text{Im}\{\Delta\epsilon F_{\text{sub}}\}$  (from the  $\delta^{-1}$  behavior at larger  $\delta$ ) and  $\text{Re}\{\Delta\epsilon F_{\text{sub}}\}$  (from the contrast at  $|\delta| \lesssim 1^{\circ}$ ), providing us the full complex value of  $\Delta\epsilon$  at an arbitrary energy.

To determine  $\Delta \epsilon$  spectroscopically, we first established the value of  $\eta$  by measuring as a function of  $\delta$  the reflected intensity from an isotropic substrate (Supporting Information). For a given sample and photon energy, we then treated Re $\{\Delta \epsilon\}$  and Im $\{\Delta \epsilon\}$  as the only free parameters, and simultaneously fit all available contrast data  $(-10^{\circ} < \delta < 10^{\circ})$ , at two different rotations  $\theta$  for each sample) to our expression for contrast with a birefringent objective (Eq. S26 of the Supporting Information). The fit quality is extremely good (solid lines, Fig. 4b,c). For both samples, the extracted values of Re $\{\Delta \epsilon\}$  and Im $\{\Delta \epsilon\}$  are nearly independent of energy, with Re $\{\Delta \epsilon\} \approx -0.6$  and  $|\text{Im}\{\Delta \epsilon\}| < 0.08$  (Fig. 4d). To get the overall scale of  $\Delta \epsilon$ , we have assumed that the anisotropic medium has a thickness d = 0.3 nm, which is a reasonable thickness for both a molecular monolayer and a graphene sheet. The negative sign of Re $\{\Delta \epsilon\}$  indicates that Re $\{\epsilon_x\}$  along the stripes is smaller than Re $\{\epsilon_y\}$  normal to the stripes.

Periodic ripples in the graphene sheet would not give rise to the predominantly real and spectrally flat anisotropy in the dielectric function that we observe. Shallow rippling would mainly affect the dielectric function by tilting the graphene sheet out of the plane: the dielectric function  $\epsilon_y^{\text{ripples}}$  measured along the periodic direction  $\hat{y}$  becomes a mixture of the in-plane  $(\epsilon_{\text{in}})$  and out-of-plane  $(\epsilon_{\text{out}})$  permittivities of flat graphene, whereas light polarized along  $\hat{x}$  remains polarized in-plane everywhere, leaving  $\epsilon_x^{\text{ripples}} = \epsilon_{\text{in}}$ . The anisotropy  $\Delta \epsilon^{\text{ripples}}$  becomes proportional to  $\epsilon_{\text{in}} - \epsilon_{\text{out}}$  times a positive real number related to the ripple geometry (Supporting Information). For 2 eV light,  $\epsilon_{\text{in}} \approx 5 + 8i$  and  $\epsilon_{\text{out}} \approx 2,^{27,28}$  yielding

 $\epsilon_{\rm in} - \epsilon_{\rm out} \approx 3 + 8i$ . Ripples should therefore produce anisotropy with a large imaginary part and a positive real part, in disagreement with our experimental value  $\Delta\epsilon \approx -0.6$ . The quantity  $\epsilon_{\rm in} - \epsilon_{\rm out}$  furthermore increases by roughly 50% as probe energy decreases from 2 eV to 1 eV, <sup>27</sup> giving  $\Delta\epsilon^{\rm ripples}$  a significant spectral dependence that is not observed in the experimental  $\Delta\epsilon$ . The magnitude of the ripple-induced anisotropy would also be too small. A sinusoidal ripple with peak-to-trough amplitude 0.1 nm and period 4 nm, for example, produces  $\Delta\epsilon^{\rm ripples} = 0.009 + 0.025i$  for 2 eV light (Supporting Information). Incorporating the effects of any uniaxial strain associated with the ripples leads to similar conclusions: strain should produce significant anisotropy in the imaginary part of the dielectric function, rather than anisotropy predominantly in the real part. <sup>29</sup> These considerations rule out periodic ripples as the source of optical anisotropy.

On the other hand, an anisotropic molecular adlayer could produce the observed optical anisotropy. The adsorbed molecules must be anisotropic, and must on average align their more polarizable axis orthogonally across the 4 nm width of the armchair-aligned columns that they collectively form. Organic molecules with straight carbon chains, such as alkanes and surfactants, readily self-assemble in exactly this way on the basal plane of graphite <sup>17–19</sup> and graphene: <sup>20–23</sup> the molecules form a monolayer of tightly packed columns—observed as stripes in AFM <sup>19</sup>—whose width (often 4 nm) is determined by the chain length. The carbon chain is perpendicular to the column axis, while the columns are aligned to the armchair axes of the underlying crystal. A calculation based on a bond polarizability model (Supporting Information) confirms that alkane molecules are most polarizable along their chain axis, and that a self-assembled alkane monolayer would produce  $Re\{\Delta\epsilon\}$  agreeing in sign and approximate magnitude with our experimental value of -0.6. Because the polarizabilities result from electronic transitions well above our probing photon energy, little spectral variation of  $\text{Re}\{\Delta\epsilon\}$  is expected, consistent with our measurements. The dielectric anisotropies of films of other oriented, organic chain molecules like polyimides<sup>30</sup> also agree in sign and magnitude with our experimental Re{ $\Delta \epsilon$ }. We conclude that an anisotropic molecular adlayer would fully explain the observed  $\Delta\epsilon$ . While organic molecules with a carbon backbone adsorb well on graphene, likely owing to lattice match, <sup>17,31</sup> smaller anisotropic molecules could also produce the observed optical anisotropy—although larger molecules more naturally explain the 4 nm period.

We have demonstrated that polarization-contrast microscopy can image the domains of stripes on graphene, which were previously observed only by slow and invasive<sup>4</sup> AFM measurements. The two approaches yield fully compatible information about the spatial character and symmetry axes of the domains. The optical method additionally provides quantitative spectroscopic data about the anisotropy of the sample; these data rule out an origin based on rippling of the graphene layer, but are fully consistent with expectations for an aligned molecular adlayer. We have shown in particular that an ordered monolayer of chain-like organic molecules would produce anisotropy with both the sign and magnitude of the measured value, and would naturally explain the nanoscale stripes observed in AFM.

The self-assembled adsorbates studied here are frequently, but not always, observed on graphene samples, and the precise conditions required for self-assembly are not fully understood. Assuming that the adsorbates are indeed organic, they could originate from a variety of sources. One possibility is that the adsorbates are airborne, perhaps arising from outgassing plastics or pump oil; this explanation is particularly attractive given that the stripes appear on samples that have not been processed following exfoliation or furnace annealing. But organic contaminants from tape residues or skin oil that are sufficiently mobile on the sample surface could also produce the self-assembled stripes. We emphasize that signatures of this self-assembly phenomenon have been observed by several groups on several different hexagonal crystals, 3-11 so the molecule or molecules responsible for this phenomenon appear to be relatively commonplace.

The noninvasiveness, simplicity, and rapid imaging capability of our optical technique should greatly facilitate future studies of the self-assembly process in controlled environments. The utility of our technique is not limited to graphene: we have observed optical anisotropy from domains of adsorbates on hBN (Supporting Information), and we expect to observe similar optical anisotropy on flakes of transition metal dichalcogenides that display stripes in AFM. <sup>11</sup> Polarization-contrast spectra collected outside the visible range should also be valuable. Mid-infrared spectra should help chemically fingerprint the aligned molecules based on vibrational modes, while near-infrared spectra may contain absorption signatures of minibands that result from the periodic potential imposed by the adsorbates. <sup>32,33</sup> We searched for such superlattice features in graphene near the characteristic energy  $hv_F/L \approx 1$  eV, where  $v_F$  is the Fermi velocity and L=4 nm is the stripe period, but found only one sample with any absorption near 1 eV (Supporting Information). Our work invites a more complete investigation of the influence of these self-assembled adsorbates on the electronic properties of two-dimensional materials.

# **Supporting Information**

Derivations of expressions for reflection contrast. Calculation of optical anisotropy for periodically rippled graphene and ordered alkane chains. Additional polarization-contrast data and fits for Sample A. Polarization-contrast images of thin hBN flakes. Polarization-contrast spectra for graphene on fused silica and discussion of possible superlattice features. Movie of polarized contrast variation under sample rotation.

## Acknowledgments

Sample fabrication, AFM measurement, and polarization-contrast microscopy using the Nikon LV100 POL were performed at the Stanford Nano Shared Facilities (SNSF) with support from the Air Force Office of Science Research (grant FA9550-16-1-0126). Use of the Nikon LV100 POL microscope was additionally supported by a seed grant from SNSF and the Stanford Dean of Research. Support for the optical measurements (YL) was provided by the Air Force Office of Scientific Research (grant FA9550-14-1-0040). Support for analysis (TH)

was provided by Department of Energy, Office of Science, Basic Energy Sciences, Materials Science and Engineering Division (contract DE-AC02-76SF00515). Growth of hexagonal boron nitride crystals (KW and TT) was supported by the Elemental Strategy Initiative conducted by the MEXT, Japan and JSPS KAKENHI Grant Numbers JP15K21722. PG acknowledges support from Prof. Charles H. Kruger and the Stanford University Office of Technology Licensing received through the Stanford Graduate Fellowship program. We thank Prof. Jen Dionne for use of a microscope and spectrometer at an early stage of this work.

### Conflict of Interest

The authors declare no competing financial interest.

#### References

- (1) Fasolino, A.; Los, J. H.; Katsnelson, M. I. Intrinsic ripples in graphene. *Nat. Mater.* **2007**, *6*, 858–861.
- (2) Lui, C. H.; Liu, L.; Mak, K. F.; Flynn, G. W.; Heinz, T. F. Ultraflat graphene. Nature 2009, 462, 339–341.
- (3) Choi, J. S.; Kim, J.-S.; Byun, I.-S.; Lee, D. H.; Lee, M. J.; Park, B. H.; Lee, C.; Yoon, D.; Cheong, H.; Lee, K. H.; Son, Y.-W.; Park, J. Y.; Salmeron, M. Friction Anisotropy-Driven Domain Imaging on Exfoliated Monolayer Graphene. *Science* **2011**, 333, 607–610.
- (4) Gallagher, P.; Lee, M.; Amet, F.; Maksymovych, P.; Wang, J.; Wang, S.; Lu, X.; Zhang, G.; Watanabe, K.; Taniguchi, T.; Goldhaber-Gordon, D. Switchable friction enabled by nanoscale self-assembly on graphene. *Nat. Commun.* 2016, 7, 10745.

- (5) Woods, C. R.; Withers, F.; Zhu, M. J.; Cao, Y.; Yu, G.; Kozikov, A.; Shalom, M. B.; Morozov, S. V.; van Wijk, M. M.; Fasolino, A.; Katsnelson, M. I.; Watanabe, K.; Taniguchi, T.; Geim, A. K.; Mishchenko, A.; Novoselov, K. S. Macroscopic self-reorientation of interacting two-dimensional crystals. *Nat. Commun.* 2016, 7, 10800.
- (6) Wastl, D. S.; Speck, F.; Wutscher, E.; Ostler, M.; Seyller, T.; Giessibl, F. J. Observation of 4 nm Pitch Stripe Domains Formed by Exposing Graphene to Ambient Air. ACS Nano 2013, 7, 10032–10037.
- (7) Lu, Y.-H.; Yang, C.-W.; Hwang, I.-S. Molecular Layer of Gaslike Domains at a Hydrophobic–Water Interface Observed by Frequency-Modulation Atomic Force Microscopy. *Langmuir* **2012**, *28*, 12691–12695.
- (8) Lu, Y.-H.; Yang, C.-W.; Fang, C.-K.; Ko, H.-C.; Hwang, I.-S. Interface-Induced Ordering of Gas Molecules Confined in a Small Space. *Sci. Rep.* **2014**, *4*, 7189.
- (9) Rastei, M. V.; Heinrich, B.; Gallani, J. L. Puckering Stick-Slip Friction Induced by a Sliding Nanoscale Contact. *Phys. Rev. Lett.* **2013**, *111*, 084301.
- (10) Sghaier, T.; Liepvre, S. L.; Fiorini, C.; Douillard, L.; Charra, F. Optical absorption signature of a self-assembled dye monolayer on graphene. *Beilstein J. Nanotechnol.* 2016, 7, 862–868.
- (11) Boland, M. J.; Nasseri, M.; Hunley, D. P.; Ansary, A.; Strachan, D. R. Striped nanoscale friction and edge rigidity of MoS<sub>2</sub> layers. *RSC Adv.* **2015**, *5*, 92165–92173.
- (12) Robinson, P. C.; Bradbury, S. *Qualitative Polarized-Light Microscopy*; Oxford Univ. Press, 1992.
- (13) Wahlstrom, E. E. Optical Crystallography, 5th ed.; Wiley, 1979.
- (14) Lefebvre, J.; Finnie, P. Polarized light microscopy and spectroscopy of individual single-walled carbon nanotubes. *Nano Res.* **2011**, 4, 788–794.

- (15) Liu, K.; Hong, X.; Zhou, Q.; Jin, C.; Li, J.; Zhou, W.; Liu, J.; Wang, E.; Zettl, A.; Wang, F. High-throughput optical imaging and spectroscopy of individual carbon nanotubes in devices. *Nat. Nanotechnol.* **2013**, *8*, 917–922.
- (16) Fang, G.; Maclennan, J. E.; Clark, N. A. High Extinction Polarimeter for the Precision Measurement of the In-Plane Optical Anisotropy of Molecular Monolayers. *Langmuir* 2010, 26, 11686–11689.
- (17) McGonigal, G. C.; Bernhardt, R. H.; Thomson, D. J. Imaging alkane layers at the liquid/graphite interface with the scanning tunneling microscope. Appl. Phys. Lett. 1990, 57, 28–30.
- (18) Rabe, J. P.; Buchholz, S. Commensurability and Mobility in Two-Dimensional Molecular Patterns on Graphite. *Science* **1991**, *253*, 424–427.
- (19) Manne, S.; Gaub, H. E. Molecular Organization of Surfactants at Solid-Liquid Interfaces. *Science* **1995**, *270*, 1480–1482.
- (20) Prado, M. C.; Nascimento, R.; Moura, L. G.; Matos, M. J. S.; Mazzoni, M. S. C.; Cancado, L. G.; Chacham, H.; Neves, B. R. A. Two-Dimensional Molecular Crystals of Phosphonic Acids on Graphene. ACS Nano 2011, 5, 394–398.
- (21) Deshpande, A.; Sham, C.-H.; Alaboson, J. M. P.; Mullin, J. M.; Schatz, G. C.; Hersam, M. C. Self-Assembly and Photopolymerization of Sub-2 nm One-Dimensional Organic Nanostructures on Graphene. J. Am. Chem. Soc. 2012, 134, 16759–16764.
- (22) Su, Y.; Han, H.-L.; Cai, Q.; Wu, Q.; Xie, M.; Chen, D.; Geng, B.; Zhang, Y.; Wang, F.; Shen, Y. R.; Tian, C. Polymer Adsorption on Graphite and CVD Graphene Surfaces Studied by Surface-Specific Vibrational Spectroscopy. *Nano Lett.* **2015**, *15*, 6501–6505.
- (23) Yu, Y.-J.; Lee, G.-H.; Choi, J. I.; Shim, Y. S.; Lee, C.-H.; Kang, S. J.; Lee, S.; Rim, K. T.; Flynn, G. W.; Hone, J.; Kim, Y.-H.; Kim, P.; Nuckolls, C.; Ahn, S.

- Epitaxially Self-Assembled Alkane Layers for Graphene Electronics. *Adv. Mater.* **2016**, 29, 1603925.
- (24) Weightman, P.; Martin, D. S.; Cole, R. J.; Farrell, T. Reflection anisotropy spectroscopy. *Rep. Prog. Phys.* **2005**, *68*, 1251–1341.
- (25) Mak, K. F.; Sfeir, M. Y.; Wu, Y.; Lui, C. H.; Misewich, J. A.; Heinz, T. F. Measurement of the Optical Conductivity of Graphene. *Phys. Rev. Lett.* **2008**, *101*, 196405.
- (26) Choi, J. S.; Chang, Y. J.; Woo, S.; Son, Y.-W.; Park, Y.; Lee, M. J.; Byun, I.-S.; Kim, J.-S.; Choi, C.-G.; Bostwick, A.; Rotenberg, E.; Park, B. H. Correlation between micrometer-scale ripple alignment and atomic-scale crystallographic orientation of monolayer graphene. Scientific Reports 2014, 4.
- (27) Cheon, S.; Kihm, K. D.; Kim, H. G.; Lim, G.; Park, J. S.; Lee, J. S. How to Reliably Determine the Complex Refractive Index (RI) of Graphene by Using Two Independent Measurement Constraints. Sci. Rep. 2014, 4, 6364.
- (28) Matthes, L.; Pulci, O.; Bechstedt, F. Influence of out-of-plane response on optical properties of two-dimensional materials: First principles approach. *Phys. Rev. B* **2016**, 94, 205408.
- (29) Pereira, V. M.; Ribeiro, R. M.; Peres, N. M. R.; Neto, A. H. C. Optical properties of strained graphene. *Europhys. Lett.* **2010**, *92*, 67001.
- (30) Boese, D.; Lee, H.; Yoon, D. Y.; Swalen, J. D.; Rabolt, J. F. Chain orientation and anisotropies in optical and dielectric properties in thin films of stiff polyimides. *J. Polym. Sci. Part B Polym. Phys.* **1992**, *30*, 1321–1327.
- (31) Groszek, A. J. Selective Adsorption at Graphite/Hydrocarbon Interfaces. *Proc. R. Soc.* A 1970, 314, 473–498.
- (32) Tsu, R. Superlattice to Nanoelectronics, 2nd ed.; Elsevier, 2011.

(33) Park, C.-H.; Yang, L.; Son, Y.-W.; Cohen, M. L.; Louie, S. G. Anisotropic behaviours of massless Dirac fermions in graphene under periodic potentials. *Nat. Phys.* **2008**, *4*, 213–217.